EFDA–JET–PR(09)16

E. Zilli, M. Brombin, A. Boboc, L. Giudicotti, A. Murari
and JET EFDA contributors

Theoretical Investigation on an Anomalous Behaviour of the Polarimetric Measurements at JET

Theoretical Investigation on an Anomalous Behaviour of the Polarimetric Measurements at JET

E. Zilli[1], M. Brombin[1,2], A. Boboc[3], L. Giudicotti[1], A. Murari[1]
and JET EFDA contributors*

JET-EFDA, Culham Science Centre, OX14 3DB, Abingdon, UK

[1]Consorzio RFX, Associazione Euratom-ENEA sulla Fusione, Corso Stati Uniti 4, 35127, Padova, Italy
[2]University of Padova, Industrial Engineering Department, via Venezia 1, 35131, Padova, Italy
[3]EURATOM-UKAEA Fusion Association, Culham Science Centre, OX14 3DB, Abingdon, OXON, UK
** See annex of F. Romanelli et al, "Overview of JET Results",*
(Proc. 22 [nd] IAEA Fusion Energy Conference, Geneva, Switzerland (2008)).

Preprint of Paper to be submitted for publication in
Journal of Optics

Abstract

The experimental data collected during the calibration of the polarimeter at JET show clear evidence of non ideal behaviour of the diagnostic optics. The influence of this non ideal behaviour on the FIR polarimetric measurements at JET is investigated, since it results in anomalies which render difficult the interpretation of the detected signals, in particular the Cotton Mouton effect. These anomalies are clearly displayed during the calibration operations in absence of plasma. In fact, when the polarization of the probing beam is rotated, the phase shift between the two detector signals for a particular chord is not constant, as expected, but it changes a lot.
After a brief introduction to the implementation of the polarimetry on JET and after a presentation of typical polarimetric signals, the optical characteristics of the recombination plate are analyzed. Their effect is studied using the classical laws of optic. The results show that the recombination plates don't look to be the cause of the detected anomalies. Then, the dielectric waveguides used to transfer the

recombined beams from the Torus Hall to the detectors are considered as the possible origin of non ideal behaviour of the diagnostic optics. Assuming that the transmission properties of the optics after the recombination plate are known, a general method to evaluate the signals at the detectors is presented, which includes the effects of the optical components in the dielectric waveguides. As a particular case, the simple rotation of the polarization acquired along the beam line from Torus to the detectors is modelled. The results obtained in this case are compared with experimental calibration data and they indicate that the anomalies present in the calibration data could be at least partly caused by changes of the polarization, due to various reasons such as non ideal components or the reflections on metal mirrors, which may produce rotations of the polarization state of the recombined beams.

1 Introduction

The JET polari-interferometer was initially designed to operate as a pure multichannel far-infrared interferometer of the Mach-Zehnder type(1). The introduction of additional optics allowed measurements of the Faraday effect and then the determination of the poloidal magnetic field distribution(2). Recently the system has been upgraded with a new set-up to allow simultaneous Faraday rotation angle and Cotton Mouton phase shift measurement(3). From the latter is possible to obtain the line integrated plasma electron density.

At JET, the Cotton Mouton effect for the measurement of the line integrated density, alternative to interferometry, has been widely investigated (4)÷(7). This new measurement, once reliable enough, could be used to alleviate the problem of the fringe jumps, which affect JET interferometric measurements. The various studies of the Cotton Mouton effect include a statistical comparison between the line integrated density from interferometry and polarimetry

over a wide range of main plasma parameters, in particular for high values of electron density taking into account data from Thomson Scattering, magnetic probes and from an equilibrium code (EFIT) (7).

Even if estimates of the electron density line integrals are available, the polarimetric diagnostic seems to be affected by anomalies, which are clearly displayed during the calibration. The source of this anomaly is still unknown but a deep analysis to understand it is underway since the anomaly makes it very difficult to analyze polarimetric data, in particular the Cotton Mouton effect. So far JET polarimetric signals have to be preprocessed using a model which includes a *"spurious ellipticity"* of the probing beam, assumed to be due to non ideal behaviuor of unidentified optical components. This spurious ellipticity has to be added to the one produced by the plasma (8) to derive meaningful measurements and it is estimated from the calibration procedure. Even if, as a result of this correction, there is a good agreement between the line integrated electron densities measured by interferometry and polarimetry, it should be noted that the correction is purely empirical and therefore not completely satisfactory. For example, an unresolved issue remains the total error on the measurements, including the effect of this correction for the spurious ellipticity. This question becomes especially crucial in case of discrepancies between the density measurements obtained from interferometry and polarimetry. It has also to be emphasised that this error could change for different plasma scenarios. It is therefore considered very important to understand the cause of this anomaly of the polarimetric data and every effort should be done to eliminate or at least to reduce the problem possibly with a suitable intervention on the diagnostic hardware.

The aim of the present work is the analysis of some optical components which could be the source of the observed anomalous behaviour of the polarimetric measurements. Of course, suitable tests will have to be performed to verify the results of this investigation.

The paper starts with a revision of the polarimetric measurements principle in JET and a presentation of the main aspects of the calibration and processed signals (Section 2). Plots of experimental calibration data for the four vertical channels, presented in Section 3, clearly show the presence of the anomaly. Assuming the recombination plate as an optical component which could introduce ellipticity in the polarization, a detailed analysis of its main optical properties and its theoretical behaviour, in accordance with the basic laws of optics, is described (Section 4). The effects of this plate on the polarimetric measurements are shown. Then, the beam transfer line from the Torus hall to the detectors, including the dielectric waveguide, mirrors, wire grids and optical elbows, is considered. Given the transmission properties of the optics after the recombination plate, a general method to evaluate the signals at the detectors is described in Section 5. At last, the effect of a simple rotation of the polarization along the beam line from Torus to the detectors is calculated and the comparison with the experimental data of the calibration is reported (Section 6).

2 Polarimetry: operation principle

A simplified scheme of the general optical set-up for one vertical chord of JET polari-interferometer is shown in Fig. 1. A reference frame is assumed

with x-axis along the toroidal direction, the y-axis along the radial direction and the z-axis along the vertical axis of the torus. The DCN ($\lambda = 195\mu m$) laser beam is split into a probing beam and a reference beam (also known as *"modulated beam"*). Neglecting the beam splitter system, which divides the beam into the different chords, each of the probing beam passes through a wire grid used as an optical filter and through an half wave plate, used for calibration and diagnostic set-up prior entering the vacuum vessel. On the vertical channels, the polarization is linear at 45° with respect to the toroidal direction (x- axis) to maximise the Cotton Mouton effect. After passing through the plasma, the polarization of the radiation experiences a rotation because of the Faraday effect and acquires ellipticity due to the Cotton Mouton effect. The input and exit windows to the vacuum chamber are made of z-cut crystal quartz.

The reference beam is modulated (frequency shifted) by a rotating grating wheel at 100kHz ($\omega_0 = 2\pi \times 10^5 s^{-1}$) and its polarisation is rotated via a half wave plate of 45°; then it is split into the different channels. Each of these beams passes through a wire grid used as an optical filter before being recombined with the probing beam by a recombination quartz plate. The recombined beam passes through an oversized dielectric waveguide (Pyrex tubes of $\sim 80mm$ inner diameter) and then it reaches a wire grid which acts as an analyser, dividing the electric field components into two direction x and y, that are focused onto two corresponding detectors.

Supposing all the optical components behave ideally, the probing beam, when passing through the plasma can be expressed in the following complex form:

$$E_x^{(p)} = E_0 \cos\Theta \tag{2.1}$$

$$E_y^{(p)} = E_0 \sin\Theta e^{-i\Phi} \tag{2.2}$$

with time dependence $e^{-i\omega t}$, $\omega = 2\pi c/\lambda$ and

$$\Theta = \Theta_0 + \alpha \tag{2.3}$$

with $\Theta_0 = 45°$.

In presence of plasma, α is due to the Faraday effect and Φ is the phase shift between the electric field components E_x and E_y due to the Cotton Mouton effect. In absence of plasma, α is produced by a rotation of the half wave plate used for the calibration. The reference beam can be expressed as:

$$E_x^{(r)} = E_{0g} \cos\Theta_g \tag{2.4}$$

$$E_y^{(r)} = E_{0g} \sin\Theta_g \tag{2.5}$$

with time dependence $e^{-i(\omega+\omega_0)t}$ and $\Theta_g = 45°$.

The calculation of the average power of the radiation incident on the detectors, evaluated over times much longer than ω^{-1} but shorter than ω_0^{-1}, leads to the following expressions for the detector signals:

$$i(t) = K_x(E_x^{(p)} E_x^{(r)*} e^{i\omega_0 t} + c.c.) \tag{2.6}$$

$$p(t) = K_y(E_y^{(p)} E_y^{(r)*} e^{i\omega_0 t} + c.c.), \tag{2.7}$$

where the signals from x-component and y-component detector are indicated as $i(t)$ (*"interferometric signal"*) and $p(t)$ (*"polarimetric signal"*) respectively, K_x and K_y are proportional to the respective detector responsivities. Inserting relations (2.1) and (2.4) into (2.6) it possible to obtain:

$$i(t) = K_x(E_0 E_{0g}^* e^{i\omega_0 t} + E_0^* E_{0g} e^{-i\omega_0 t}) \cos\Theta \cos\Theta_g. \tag{2.8}$$

Writing

$$E_0 = |E_0| e^{-i\phi_p}, \quad E_{0g} = |E_{0g}| e^{-i\phi_g}, \quad \Delta\phi = \phi_p - \phi_g \tag{2.9}$$

the previous relation can be expressed as

$$i(t) = K_x \sqrt{2} |E_o| |E_{0g}| \cos\Theta \cos(\omega_0 t - \Delta\phi). \tag{2.10}$$

The phase shift $\Delta\phi$, which accounts for the different optical path between probing and reference beam and for the electron density effect on the probing signal phase, is not important for polarimetry. It can be omitted by the suitable choice of the time-line origin. A similar expression for $p(t)$ is obtained, inserting the relations (2.2) and (2.5) into (2.7). Finally the detector signals can be written in the form:

$$i(t) = A_i \cos \omega_0 t \tag{2.11}$$

$$p(t) = A_p \cos(\omega_0 t - \varphi) \tag{2.12}$$

where

$$A_i = A \cos \Theta \tag{2.13}$$

$$A_p = B \sin \Theta \tag{2.14}$$

$$A = K_x \sqrt{2} |E_0||E_{0g}| \tag{2.15}$$

$$B = K_y \sqrt{2} |E_0||E_{0g}| \tag{2.16}$$

$$\varphi = \phi_0 + \Phi, \tag{2.17}$$

where ϕ_0 is the phase shift between the two signals without plasma. It is zero just in this particular context, but generally it is not zero, as it will be further shown. The detector outputs are electronically acquired with a time resolution of 1ms up to 14 ms depending on the acquisition set-up and they are processed by analog phase sensitive electronic cards to obtain the following four signals:

$$RMS = \langle i(t) \cdot i(t) \rangle = \frac{1}{2} A_i^2 \tag{2.18}$$

$$PSD = \langle i(t) \cdot p(t) \rangle = \frac{1}{2} A_i A_p \cos\varphi \tag{2.19}$$

$$RMS' = \langle i'(t) \cdot i'(t) \rangle = \frac{1}{2} A_i'^2 \tag{2.20}$$

$$PSD' = \langle i'(t) \cdot p(t) \rangle = \frac{1}{2} A_i' A_p \sin\varphi \tag{2.21}$$

where $i'(t) \sim \sin \omega_0 t$ is generated by 90° phase shifting $i(t)$ and its amplitude A_i' is assumed different from A_i. From these four relations the following ratios can be calculated:

$$R = \frac{PSD}{RMS} = \frac{A_p}{A_i} \cos\varphi \tag{2.22}$$

$$R' = \frac{PSD'}{\sqrt{RMS \cdot RMS'}} = \frac{A_p}{A_i} \sin\varphi. \tag{2.23}$$

If the relations (2.13) and (2.14) are satisfied, the previous ratios can be rewritten as:

$$R = C^{-1} \tan\Theta \cos\varphi \tag{2.24}$$

$$R' = C^{-1} \tan\Theta \sin\varphi \tag{2.25}$$

defining

$$C = \frac{A}{B}. \tag{2.26}$$

Given the two ratios R and R', the angles Θ and Φ can be easily obtained. In fact, their ratio gives:

$$\varphi = \arctan\left(\frac{R'}{R}\right), \tag{2.27}$$

independent from Θ, and then the Cotton Mouton phase difference

$$\Phi = \varphi - \phi_0. \tag{2.28}$$

The sum of their squares leads to:

$$\Theta = \arctan(C\sqrt{R^2 + R'^2}) \tag{2.29}$$

without any dependence on φ. The two calibration constants ϕ_0 and C are determined in absence of plasma, when $\Phi = 0$ and $\Theta = 45°$. In this treatment, it is assumed that the phase shift without plasma $\varphi = \phi_0$ is independent from the Faraday rotation and therefore it remains constant during the scan of α performed to calibrate the diagnostic.

The angles Θ and Φ define the polarization state of the radiation exiting the plasma. In fact, the Stokes vector components can be evaluated as:

$$s_1 = \cos 2\Theta \tag{2.30}$$

$$s_2 = \sin 2\Theta \cos \Phi \tag{2.31}$$

$$s_3 = \sin 2\Theta \sin \Phi \tag{2.32}$$

with $0 \leq \Theta \leq 90°$ and $-180° \leq \Phi \leq 180°$. By these expressions it is possible to calculate the main polarization parameters: ellipticity ϵ, defined as the ratio between minor and major axes of the polarization ellipse, and ψ, the tilt angle of the polarization ellipse with respect to the x-direction

$$\epsilon = \frac{|s_3|}{1 + \sqrt{1 - s_3^2}}, \tag{2.33}$$

$$\psi = \frac{1}{2} \arctan\left(\frac{s_2}{s_1}\right) \qquad (0 \leq \psi \leq 180°). \tag{2.34}$$

The Faraday rotation angle is given by:

$$\Psi = \psi - \Theta_0, \tag{2.35}$$

it is equal to $\alpha = \Theta - \Theta_0$ only in absence of ellipticity ($\Phi = 0$).

3 Calibration and data processing

At JET an on-line calibration is routinely performed before each JET pulse, rotating the polarization direction of the probing beam by a known angle α using the half wave plate. Calibration examples are reported in figures 2÷5 for the vertical channels 1÷4 respectively. The R and R' curves, coming from experimental data through (2.22) and (2.23), are plotted as functions of the angle α and the phase shift φ, calculated by (2.27), is also shown. It is clear that the angle φ (in this case it is equal to ϕ_0) is not constant for a variation of the angle α (and so of Θ). This behaviour completely contravenes the assumptions of the theoretical treatment previously described and it makes

difficult the interpretation of the polarimetric measurements.

Because of this non ideal behaviour, at JET the polarimetric signals are processed using a model which assumes that an unspecified optical element generates an additional ellipticity (*"spurious ellipticity"*) characterized by a constant phase shift $\tilde{\phi}$ referred to a rotated co-ordinate system of unknown orientation Ξ (8). Optimizing four parameters by the least square method, the R and R' values, evaluated with this model in absence of plasma, fit very well the experimental calibration curves, obtained varying α. In presence of plasma, using the parameters optimized during the calibration, the processing system evaluates on line the Θ and Φ angles and other polarization parameters. In particular the Φ angle allows the calculation of the line integrated plasma electron density which usually agrees with the one provided by interferometry. This comparison is still under investigation. Fig. 6 shows the evolution during one shot of Φ and Ψ angles evaluated by this algorithm for channel 3, and these two parameters are compared with the experimental phase shift φ of the two detector signals. The difference between the Cotton Mouton angle Φ obtained from the algorithm and the phase shift φ, given directly by the raw data, is large (a factor of five) even if the Faraday rotation is small ($\sim 1^{\circ}$). This confirms that a numerical postprocessing of data is needed until the anomaly is understood and fixed or almost completely reduced. Any tentative to evaluate Φ directly from φ, given by the raw data, would cause significant errors. The difference between Φ and φ is indeed large even for small Faraday angles.

Nevertheless the use of this postprocessing algorithm at JET is justified only by a qualitative agreement between the measurements of the line integrated

plasma electron density by polarimetry and interferometry, but its reliability hasn't been quantified. Moreover it hasn't been demonstrated that the agreement between the R, R' and φ values given by the model with the experimental ones in absence of plasma is still verified in presence of plasma. Indications about the reliability of the measurement of the line integrated plasma electron density by polarimetry using the Cotton Mouton effect, have been obtained by statistical analysis (4)-(7). In particular in (7) it has been shown that the agreement between the interferometric and polarimetric measurement of the electron density is within $1.143 \times^{19} \mathrm{m}^{-2}$, for the entire range of densities, in more than 90% of cases considered in that work. The shots belong to various campaigns in the years 2006 and 2007, and they were selected to produce statistics without any particular bias linked to particular experiments. This agreement is very good (99%) for densities higher than $20 \times^{19} \mathrm{m}^{-2}$.

4 The effect of the recombination plate

The recombination plate is a z-cut natural crystal quartz plate with thickness $h = 1.894\mathrm{mm} \pm 1\mu\mathrm{m}$. The incidence angle of both the probing and the reference beams is $\theta_0 = 45°$. The x and y directions are perpendicular and parallel with respect to the incidence plane. The electric field components corresponding to the probing and the reference beams, are partially transmitted and partially reflected by the plate, and they experience the following changes:

$$E_x'^{(p)} = P_\perp E_x^{(p)} \tag{4.1}$$

$$E_y'^{(p)} = P_\parallel E_y^{(p)} \tag{4.2}$$

$$E_x'^{(r)} = R_\perp E_x^{(r)} \tag{4.3}$$

$$E_y'^{(r)} = R_\parallel E_y^{(r)} \tag{4.4}$$

where the complex coefficients $P_\perp$, $P_\parallel$, $R_\perp$, $R_\parallel$, independent from Θ and Φ, are evaluated considering multiple reflections on the surfaces of the plate (9). The birefringence of the medium is characterised by two refraction index values: ordinary and extraordinary. The former for the electric field component E_x perpendicular to the incidence plane and the latter for the electric field component E_y parallel to the incidence plane. For $\lambda = 195\mu$m, the crystal quartz has an ordinary refraction index $n_0 = 2.112$ and an extraordinary refraction index $n_s = 2.156$, for a propagation perpendicular to the optical axis (10). Then, assuming that E_x is associated to the ordinary refraction index $n_\perp = n_0$ and E_y is associated to the extraordinary one, evaluated taking into account of the angle between the refracted beam and the optical axis

$$n_\parallel = \sqrt{n_0^2 + \left(1 - \frac{n_0^2}{n_s^2}\right) \sin^2 \theta_0}. \tag{4.5}$$

Neglecting dielectric losses, the complex coefficients in (4.1) $\div$ (4.4) can be

expressed as:

$$P_\perp = \frac{1-\Re_\perp}{1-\Re_\perp e^{i\delta_\perp}} \qquad P_\parallel = \frac{1-\Re_\parallel}{1-\Re_\parallel e^{i\delta_\parallel}} \tag{4.6}$$

$$R_\perp = \frac{\left(1-e^{i\delta_\perp}\right)\sqrt{\Re_\perp}}{1-\Re_\perp e^{i\delta_\perp}} \qquad R_\parallel = \frac{\left(1-e^{i\delta_\parallel}\right)\sqrt{\Re_\parallel}}{1-\Re_\parallel e^{i\delta_\parallel}} \tag{4.7}$$

where

$$\Re_\perp = \frac{\sin^2(\theta_0-\theta_\perp)}{\sin^2(\theta_0+\theta_\perp)} \qquad \Re_\parallel = \frac{\tan^2(\theta_0-\theta_\perp)}{\tan^2(\theta_0+\theta_\perp)} \tag{4.8}$$

$$\delta_\perp = \frac{4\pi}{\lambda} n_\perp h\cos\theta_\perp \qquad \delta_\parallel = \frac{4\pi}{\lambda} n_\parallel h\cos\theta_\parallel \tag{4.9}$$

$$\theta_\perp = \arcsin\left(\frac{\sin\theta_0}{n_\perp}\right) \qquad \theta_\parallel = \arcsin\left(\frac{\sin\theta_0}{n_\parallel}\right). \tag{4.10}$$

It is assumed that the probing beam transmitted through the plate is still described by (2.1) and (2.2), while the reference beam is represented by

$$E_x^{(r)} = E_{0g}\cos\Theta_g \tag{4.11}$$

$$E_y^{(r)} = E_{0g}\sin\Theta_g e^{-i\phi_r} \tag{4.12}$$

to account for a possible spurious ellipticity due to reflection on metal surfaces and crossing a beamsplitter system. So, using the notations

$$P_{\perp,\parallel} = \left|P_{\perp,\parallel}\right| e^{i\psi_{\perp,\parallel}} \qquad R_{\perp,\parallel} = \left|R_{\perp,\parallel}\right| e^{i\phi_{\perp,\parallel}} \tag{4.13}$$

and inserting equations (2.1), (2.2), (4.11) and (4.12) into (4.1) $\div$ (4.4), neglecting the prime sign, it is possible to write the equations for the beams

outcoming from the recombination plate as follows:

$$E_x^{(p)} = |P_\perp| \, e^{i\psi_\perp} \cdot E_0 \cos\Theta \tag{4.14}$$

$$E_y^{(p)} = \left|P_\parallel\right| e^{i\psi_\parallel} \cdot E_0 \sin\Theta e^{-i\Phi} \tag{4.15}$$

$$E_x^{(r)} = |R_\perp| \, e^{i\phi_\perp} \cdot E_{0g} \cos\Theta_g \tag{4.16}$$

$$E_y^{(r)} = \left|R_\parallel\right| e^{i\phi_\parallel} \cdot E_{0g} \sin\Theta_g e^{-i\phi_r}. \tag{4.17}$$

Explicit expressions for the moduli and the phases of $P_{\perp,\parallel}$ and $R_{\perp,\parallel}$ are reported in the Appendix A. Using these mathematical relations it is easy to calculate the ellipticity introduced on the two beams (probing and reference) by the recombination plate, supposing they are initially linearly polarized at 45° ($\Theta = 45°$, $\Phi = 0$, $\phi_r = 0$). So the polarization ellipse of the reference beam has ellipticity $\epsilon_r = 0.214$ and tilt angle $\psi_r = 20.41°$ with respect to the x-direction. On the other hand the polarization ellipse of the probing beam has ellipticity $\epsilon_p = 0.056$ and tilt angle $\psi_p = 144.46°$. The effect of the recombination plate on the polarization of the beams is not only a modification of the ellipticity but also a rotation of the polarization ellipse such that the final angle is very far from the initial 45°.

If the recombined beam is transferred unchanged to the detection system and the x and y electric field components reach the respective detectors without any interference between them, the signals at the detectors can be evaluated as previously seen in Section 2, putting the relations (4.14) ÷ (4.17) into (2.6) and (2.7). The expressions (2.11) and (2.12) are again satisfied; the

amplitudes A_i and A_p can be written in the form (2.13) and (2.14) with

$$A = K_x\sqrt{2}\,|P_\perp|\,|R_\perp|\,|E_0|\,|E_{0g}| \tag{4.18}$$

$$B = K_y\sqrt{2}\,\left|P_\parallel\right|\,\left|R_\parallel\right|\,|E_0|\,|E_{0g}| \tag{4.19}$$

and the relation (2.17) for φ is still true with

$$\phi_0 = \psi_\perp - \psi_\parallel - \phi_\perp + \phi_\parallel - \phi_r. \tag{4.20}$$

The two angles Θ and Φ can be evaluated using the signal processing method exposed in Section 2. With respect to the ideal case, only the two calibration constants C and ϕ_0 are different, and the rest doesn't vary.
The analysis proposed in this section allows to conclude that:

1. the recombination plate modifies considerably the polarization state of both the probing and the reference beam;

2. anyway, this doesn't affect the polarimetric measurements of Θ and Φ, the effects of the recombination plate on the polarization state of the beams are compensated by the calibration. In particular, the phase shift φ should remain constant in absence of plasma, when α is varied;

3. if the reference beam had some ellipticity, it would be corrected by the calibration.

Note that the main reported conclusions are independent from the numerical values of the four complex coefficients $P_\perp, P_\parallel, P_\perp, P_\parallel$ which determine the transmission and reflection properties of the plate.

5 The dielectric waveguide

The dielectric waveguide used to transfer the recombined beam from the recombination plate to the detectors is not a straight single Pyrex tube but a rather complex optical system with other optics, including mirrors. Let's suppose that:

1. the x and y electric field components are still perpendicular or parallel with respect to the planes of incidence of the reflective surfaces, along the path between the recombination plate and the detection section;

2. all the other optics of the beam transfer line, included the wire grid in front of the detectors, behave ideally.

Then, without making any numeric calculation, it is possible to say that the E'_x and E'_y electric field components reaching respectively the x and y detectors are proportional to the initial E_x and E_y components by the mean of complex coefficients. This can be expressed by the use of a diagonal matrix:

$$\begin{pmatrix} E'_x \\ E'_y \end{pmatrix} = \begin{pmatrix} T_{xx} & 0 \\ 0 & T_{yy} \end{pmatrix} \cdot \begin{pmatrix} E_x \\ E_y \end{pmatrix} \tag{5.1}$$

where T_{xx} and T_{yy} are complex coefficients to be determined. The polarization states of the beam will be further modified with respect to the changes introduced by the recombination plate. The calculation of the signals at the detectors would lead to the same conclusions as in Section 4; the procedure explained in Section 2 should be still reliable as long as the calibration constants C and ϕ_0 are adjusted by the calibration procedure. In particular the

phase shift φ between the two signals should be constant for a scan of the angle α during the calibration without plasma, which actually doesn't occur. If instead, for any reason, the x and y detectors are not reached only by the E_x and E_y field components respectively, but by a combination of the two, then a non diagonal matrix should be used instead of (5.1) to calculate the signals:

$$\begin{pmatrix} E'_x \\ E'_y \end{pmatrix} = \begin{pmatrix} T_{xx} & T_{xy} \\ T_{yx} & T_{yy} \end{pmatrix} \cdot \begin{pmatrix} E_x \\ E_y \end{pmatrix}. \tag{5.2}$$

This formalism is more general and allows modelling other additional effects, for example a non ideal behaviour of the wire grid in front of the detectors which could have finite transmission and reflection coefficients for electric field parallel and perpendicular to the wires respectively. Writing

$$T_{jk} = |T_{jk}|\, e^{i\phi_{jk}} \qquad\qquad (\mathrm{j},\mathrm{k}) = (\mathrm{x},\mathrm{y}), \tag{5.3}$$

the electric field components E_x and E_y coming out from the recombination plate (4.14) $\div$ (4.17) are inserted into (5.2); the E'_x and E'_y components so evaluated can be put into (2.6) and (2.7) to calculate the detector signals. The calculus, reported in Appendix B, provides relations still in the form (2.11) and (2.12), where the amplitudes A_i and A_p and the phase shift φ are

given by:

$$A_i = A\sqrt{\left(\sum_{k=1}^{4} a_k \cos\alpha_k\right)^2 + \left(\sum_{k=1}^{4} a_k \sin\alpha_k\right)^2} \tag{5.4}$$

$$A_p = B\sqrt{\left(\sum_{k=1}^{4} b_k \cos\beta_k\right)^2 + \left(\sum_{k=1}^{4} b_k \sin\beta_k\right)^2} \tag{5.5}$$

$$\varphi = \arctan\frac{\sum_{k=1}^{4} b_k \sin\beta_k}{\sum_{k=1}^{4} b_k \cos\beta_k} - \arctan\frac{\sum_{k=1}^{4} a_k \sin\alpha_k}{\sum_{k=1}^{4} a_k \cos\alpha_k} \tag{5.6}$$

where A and B are given by (2.15) and (2.16) respectively, and the coefficients a_k and b_k (k=1,2,3,4) depend on Θ and the angles α_k and β_k depend on Φ and ϕ_r. Their explicite expressions are given by relations (B.3) $\div$ (B.18) reported in Appendix B.

The signals i(t) and p(t) at the detectors are processed to calculate the averaged out values, as in relations (2.18) $\div$ (2.21). The ratios R and R' still defined by (2.22) $\div$ (2.23), are now evaluated by the relations (5.4) $\div$ (5.6) for A_i A_p and φ. Note that their dependence on Θ and φ is very different from the one of the relations (2.24) and (2.25). In conclusion, assuming a transformation of the type (5.2), it is possible to state that:

1. the angles Θ and Φ can't be obtained from the R and R' measured values in a simple way, as it happens when the relations (2.28) and (2.29) are valid;

2. there is no direct relation between φ and Φ; now φ depends in a complex

way on Θ and Φ, as it is shown in (5.6) taking into account (B.3) $\div$ (B.18);

3. during the calibration with $\Phi = 0$ it has to be expected that the angle φ isn't constant as Θ (or α) varies, but it changes with a complex law.

As a consequence, if the waveguide system existing at JET actually operates a transformation of the type (5.2) on the field components, an algorithm to get Θ and Φ starting from given R' and R appears difficult to devise.
In addition, any possible ellipticity of the reference beam expressed by ϕ_r would not be compensated by the calibration and it would affect the accuracy of the final results. Fortunately, in the polarimeter at JET for each channel, it has been mounted a wire grid on the path of the reference beam before the recombination plate to guarantee a linear polarization, as previously said in Section 2.

6 A particular case

Among the optics included into the transfer beam line an important role is played by 90° elbows and focalizing mirrors, where reflections on metal surfaces occur. It is well-known that a radiation reflecting on a metal surface could experience a modification of its polarization. In fact the electric field components $E_\perp$ and $E_\parallel$, perpendicular and parallel to the plane of incidence, behaves differently, as well as in the case of dielectric plates (9). The result

can be expressed in the form:

$$E_{\perp}^{(r)} = \rho_{\perp} E_{\perp}^{(i)} \tag{6.1}$$

$$E_{\parallel}^{(r)} = \rho_{\parallel} E_{\parallel}^{(i)}, \tag{6.2}$$

with

$$\rho_{\perp} = -\frac{\sin(\theta_i - \theta_t)}{\sin(\theta_i + \theta_t)} \qquad \rho_{\parallel} = \frac{\tan(\theta_i - \theta_t)}{\tan(\theta_i + \theta_t)} \tag{6.3}$$

$$\sin\theta_t = \frac{1}{\hat{n}} \sin\theta_i \tag{6.4}$$

where θ_i is the angle of incidence and θ_t plays the role of a complex refraction angle. The complex refraction index can be approximated (with $\sigma \gg \omega\epsilon_0$) as

$$\hat{n} \cong (1+i)\sqrt{\frac{\mu_r \sigma}{2\omega\epsilon_0}}, \tag{6.5}$$

where σ and μ_r are respectively the conductivity and the relative magnetic permeability of the metal. For high conductivity metal as aluminium, copper or silver and for FIR wavelengths, the modulus of the refraction index is big, so that it results with a good approximation:

$$\rho_{\perp} \approx -1 \qquad \rho_{\parallel} \approx 1. \tag{6.6}$$

As consequence, a linearly polarized radiation incident with electric field tilted at an angle θ with respect to the plane of incidence, will come out tilted at $-\theta$, so it will suffer a rotation of an angle 2θ by the effect of the reflection. Then the metal surface behaves like an half wave plate with optical

axis parallel to the plane of incidence.

Then let's analyze the case that the only effect of the optical waveguide system is a rotation of an angle γ of the radiation propagating along it. The electric field components change as:

$$\begin{pmatrix} E'_x \\ E'_y \end{pmatrix} = \begin{pmatrix} \cos\gamma & \sin\gamma \\ -\sin\gamma & \cos\gamma \end{pmatrix} \cdot \begin{pmatrix} E_x \\ E_y \end{pmatrix} . \tag{6.7}$$

As shown in Section 5, the calculus of the detector signals i(t) and p(t) leads back to the relations (2.11) and (2.12), with expressions formally equal to (5.4) $\div$ (5.6) for A_i , A_p and φ where now $a_k, b_k, \alpha_k, \beta_k$ (k=1,2,3,4) are given by relations (C.1) $\div$ (C.12) reported in Appendix C.

Attempts have been done to state if curves of φ as function of $\alpha = \Theta - \Theta_0$, with $\Phi = 0$, evaluated using (5.6) with (C.1) $\div$ (C.12), could reproduce the experimental calibration curves shown in figures 2 $\div$ 5, with $\Phi = 0$ and suitable choices for γ and ϕ_r.

A particularly good agreement has been found between data calculated for $\gamma = -29^\circ$ and $\phi_r = 3^\circ$ and the experimental data for channel 3, as it can be seen in Fig. 7, where the curve of $\tan\varphi$ is compared with the experimental curve of R'/R. This agreement has been reached optimizing the values of γ and ϕ_r and the reported values are the results of the optimization. The agreement shown in Fig. 7 is very interesting because it demostrates that any possible rotation of the polarization of the radiation propagating along the waveguide up to the detectors, could be a source of the anomaly affecting the polarimetric measurements at JET. As previously shown, rotations

of the polarization could actually happen in reflections on metal mirrors. It is understood this cause of the anomaly wasn't considered for the JET polarimeter up to now.

Moreover, the fact that the agreement is optimized with a small ϕ_r angle different from zero, could be ascribed to some ellipticity of the polarization of the reference beam, perhaps due to a non perfect filtering of the wire grid.

7 Conclusions

The main results of the analysis so far developed can be summarized as follows:

1. the recombination plates don't look to be the source of the anomaly noticed in the polarimetric data at JET; they modify the polarization of the beam but these changes should be compensated by the calibration;

2. the anomaly could be ascribed to a non standard behaviour of some optical element encountered by the probing beam along its path;

3. the anomaly may be due also to changes of the polarization suffered along the optical beam line which transfers the recombined beams from the Torus hall to the detectors. The particular case of a simple rotation of the polarization proves to be very significant.

In order to carry on this investigation on the causes of the anomaly, it is necessary to go on two directions. One way is doing bench tests on all the optical components (or combinations of optics) crossed by the probing beam from the halfwave plates to the recombination plates, i.e. quartz windows,

mylar foils, TPX windows,... It is necessary to have a laser source, producing a linearly polarised beam, followed by a rotatable half wave plate and a device able to measure the polarisation state of the beam outcoming from the sample. It must be verified whether the beam crossing the sample suffers an ellipticity and how this ellipticty varies with the change of the orientation of the incident polarisation. The other way is doing a careful inspection on the paths of the beams from the recombination plates up to the detectors. The main purpose of this inspection is to obtain a precise characterisation of all the optics crossed by the beams and to draw a tridimensional map of the paths. In this way, it will be possible to properly simulate the behaviour of the beams while they travel along this section of the diagnostic. Once all these data will be available it will be possible to recognise without doubt the causes of the anomalous behaviour of the polarimeter operating at JET. It should be also possible to formulate models suitable to simulate the operation of the polarimeter. In particular, reproducing the experimental curves of φ and of the associated parameters according with α varying, as shown in figures 2÷5. When this goal will be achieved, the next step will be to define the changes which have to be perfomed on the polarimeter to remove the anomaly.

8 Acknowledgments

The authors would like to thank R. Pasqualotto for his useful and interesting suggestions. This work, supported by the European communities under the contract of association between EURATOM and ENEA, was carried out

within the framework of the European Fusion Development Agreement. The views and opinions expressed herein do not necessarily reflect the views of the European Commission.

A Transmission and reflection coefficients of the recombination plate expressed in polar form

The following relations have to be known to be able to express the coefficients given by (4.6) and (4.7) in the form (4.13):

$$|P_\perp| = \frac{|1-\Re_\perp|}{\sqrt{1+\Re_\perp^2-2\Re_\perp\cos\delta_\perp}} \tag{A.1}$$

$$|P_\parallel| = \frac{|1-\Re_\parallel|}{\sqrt{1+\Re_\parallel^2-2\Re_\parallel\cos\delta_\parallel}} \tag{A.2}$$

$$|R_\perp| = \frac{2\sqrt{\Re_\perp}\left|\sin\frac{\delta_\perp}{2}\right|}{\sqrt{1+\Re_\perp^2-2\Re_\perp\cos\delta_\perp}} \tag{A.3}$$

$$|R_\parallel| = \frac{2\sqrt{\Re_\parallel}\left|\sin\frac{\delta_\parallel}{2}\right|}{\sqrt{1+\Re_\parallel^2-2\Re_\parallel\cos\delta_\parallel}} \tag{A.4}$$

$$\psi_\perp = \arctan\left(\frac{\Re_\perp\sin\delta_\perp}{1-\Re_\perp\cos\delta_\perp}\right) \tag{A.5}$$

$$\psi_\parallel = \arctan\left(\frac{\Re_\parallel\sin\delta_\parallel}{1-\Re_\parallel\cos\delta_\parallel}\right) \tag{A.6}$$

$$\phi_\perp = \arctan\left(-\frac{1-\Re_\perp}{1+\Re_\perp}\frac{\sin\delta_\perp}{1-\cos\delta_\perp}\right) \tag{A.7}$$

$$\phi_\parallel = \arctan\left(-\frac{1-\Re_\parallel}{1+\Re_\parallel}\frac{\sin\delta_\parallel}{1-\cos\delta_\parallel}\right) \tag{A.8}$$

B Evaluation of detector signals assuming the transformation law (5.2)

Making the operation previously presented, the two signals $i(t)$ and $p(t)$ are represented by a four terms sum:

$$i(t) = K_x\sqrt{2}\,|E_0|\,|E_{0g}|\sum_{k=1}^{4} a_k \cos(\omega_0 t - \alpha_k) \tag{B.1}$$

$$p(t) = K_y\sqrt{2}\,|E_0|\,|E_{0g}|\sum_{k=1}^{4} b_k \cos(\omega_0 t - \beta_k) \tag{B.2}$$

where

$$a_1 = |T_{xx}|^2 |P_\perp| |R_\perp| \cos\Theta \tag{B.3}$$

$$a_2 = |T_{xx}| |T_{xy}| |P_\perp| \left|R_\parallel\right| \cos\Theta \tag{B.4}$$

$$a_3 = |T_{xx}| |T_{xy}| \left|P_\parallel\right| |R_\perp| \sin\Theta \tag{B.5}$$

$$a_4 = |T_{xy}|^2 \left|P_\parallel\right| \left|R_\parallel\right| \sin\Theta \tag{B.6}$$

$$b_1 = |T_{yx}|^2 |P_\perp| |R_\perp| \cos\Theta \tag{B.7}$$

$$b_2 = |T_{yx}| |T_{yy}| |P_\perp| \left|R_\parallel\right| \cos\Theta \tag{B.8}$$

$$b_3 = |T_{yy}| |T_{yx}| \left|P_\parallel\right| |R_\perp| \sin\Theta \tag{B.9}$$

$$b_4 = |T_{yy}|^2 \left|P_\parallel\right| \left|R_\parallel\right| \sin\Theta \tag{B.10}$$

$$\alpha_1 = -\psi_\perp + \phi_\perp \tag{B.11}$$

$$\alpha_2 = -\phi_{xx} + \phi_{xy} - \psi_\perp + \phi_\parallel - \phi_r \tag{B.12}$$

$$\alpha_3 = \phi_{xx} - \phi_{xy} - \psi_\parallel + \phi_\perp + \Phi \tag{B.13}$$

$$\alpha_4 = -\psi_\parallel + \phi_\parallel - \phi_r + \Phi \tag{B.14}$$

$$\beta_1 = -\psi_\perp + \phi_\perp \tag{B.15}$$

$$\beta_2 = -\phi_{yx} + \phi_{yy} - \psi_\perp + \phi_\parallel - \phi_r \tag{B.16}$$

$$\beta_3 = -\phi_{yy} + \phi_{yx} - \psi_\parallel + \phi_\perp + \Phi \tag{B.17}$$

$$\beta_4 = -\psi_\parallel + \phi_\parallel - \phi_r + \Phi. \tag{B.18}$$

Then, equations (B.1) and (B.2) can be expressed in the form

$$i(t) = A_i \cos(\omega_0 t - \psi_i) \tag{B.19}$$

$$p(t) = A_p \cos(\omega_0 t - \psi_p) \tag{B.20}$$

with

$$A_i = A\sqrt{\left(\sum_{k=1}^{4} a_k \cos\alpha_k\right)^2 + \left(\sum_{k=1}^{4} a_k \sin\alpha_k\right)^2} \tag{5.4}$$

$$A_p = B\sqrt{\left(\sum_{k=1}^{4} b_k \cos\beta_k\right)^2 + \left(\sum_{k=1}^{4} b_k \sin\beta_k\right)^2} \tag{5.5}$$

$$\psi_i = \arctan \frac{\sum_{k=1}^{4} a_k \sin\alpha_k}{\sum_{k=1}^{4} a_k \cos\alpha_k} \tag{B.21}$$

$$\psi_p = \arctan \frac{\sum_{k=1}^{4} b_k \sin\beta_k}{\sum_{k=1}^{4} b_k \cos\beta_k}. \tag{B.22}$$

A and B are given by relations (2.15) and (2.16) respectively. Finally, equations (5.4) and (5.5) can be put in the form (2.11) and (2.12) with

$$\varphi = \psi_p - \psi_i. \tag{B.23}$$

Equations (B.21), (B.22) and (B.23) lead to (5.6).

C Evaluation of detectors signals assuming the transformation law (6.7)

With a method similar to the previous one, for the quantities A_i, A_p and φ, it is possible to obtain relations formally equal to (5.4) $\div$ (5.6), where a_k, b_k, α_k, β_k $(k = 1, 2, 3, 4)$ are provided by:

$$a_1 = \cos^2\gamma\,|P_\perp|\,|R_\perp|\cos\Theta \tag{C.1}$$

$$a_2 = \cos\gamma\sin\gamma\,|P_\perp|\,\left|R_\parallel\right|\cos\Theta \tag{C.2}$$

$$a_3 = \cos\gamma\sin\gamma\,\left|P_\parallel\right|\,|R_\perp|\sin\Theta \tag{C.3}$$

$$a_4 = \sin^2\gamma\,\left|P_\parallel\right|\,\left|R_\parallel\right|\sin\Theta \tag{C.4}$$

$$b_1 = \sin^2\gamma\,|P_\perp|\,|R_\perp|\cos\Theta \tag{C.5}$$

$$b_2 = -\cos\gamma\sin\gamma\,|P_\perp|\,\left|R_\parallel\right|\cos\Theta \tag{C.6}$$

$$b_3 = -\cos\gamma\sin\gamma\,\left|P_\parallel\right|\,|R_\perp|\sin\Theta \tag{C.7}$$

$$b_4 = \cos^2\gamma\,\left|P_\parallel\right|\,\left|R_\parallel\right|\sin\Theta \tag{C.8}$$

$$\alpha_1 = \beta_1 = -\psi_\perp + \phi_\perp \tag{C.9}$$

$$\alpha_2 = \beta_2 = -\psi_\perp + \phi_\parallel - \phi_r \tag{C.10}$$

$$\alpha_3 = \beta_3 = -\psi_\parallel + \phi_\perp + \Phi \tag{C.11}$$

$$\alpha_4 = \beta_4 = -\psi_\parallel + \phi_\parallel - \phi_r + \Phi. \tag{C.12}$$

REFERENCES

[1]. D. Véron, Large infrared light interferometer for JET,Workshop on Diagnostics for Fusion Reactor Conditions, Varenna (Italy) 1982, **282**, C.E.C., Brussels (Belgium).

[2]. G. Braithwaite, N. Gottardi, G. Magyar, J. O'Rourke, J. Ryan, D. Véron, Review Scientific Instruments **60**, 2825 (1989).

[3]. A. Boboc, L. Zabeo, A. Murari, and JET EFDA Contributors, Review Scientific Instruments **77**, 10F324 (2006).

[4]. F. Orsitto, L. Zabeo, E. Giovannozzi, P. Buratti, and JET EFDA Contributors, Polarimetric measurements of line-integrated electron density at JET based on Cotton-Mouton effect in presence of large Faraday rotation, 47th Annual Meeting of the Division of Plasma Physics, APS, Denver 26 October 2005, L03.00003.

[5]. C. Mazzotta, F. Orsitto, A. Boboc, E. Giovannozzi, M. Brombin, A. Murari, O. Tudisco, L. Zabeo, and JET EFDA contributors, Models Comparison for JET Polarimeter Data, Proceedings of the International Workshop on Burning Plasma Diagnostics, Villa Monastero, Varenna, Italy, 24 28 September 2007.

[6]. M. Brombin, A. Boboc, C. Mazzotta, L. Zabeo, A. Murari, F. Orsitto, E. Zilli, L. Giudicotti, and JET EFDA contributors, The line-integrated plasma density from both interferometry and polarimetry at JET, 34th EPS Conference on Plasma Physics, Warsaw (2007), ECA 31F, P-2.144 (2007).

[7]. M. Brombin, A. Boboc, A. Murari, E. Zilli, L. Giudicotti, and JETEFDA Contributors, Systematic comparison between line integrated densities measured with interferometry and polarimetry at JET, Review Scientific Instruments **80**, 063506 (2009).

[8]. K. Guenther and JET-EFDA contributors, Complete far-infrared polarimetry measurements at JET, 31st Conference on Plasma Physics, London, P5-172 (2004).

[9]. M. Born and E. Wolf, Principles of Optics, Pergamon Press, Oxford, 1980.

[10]. E.E. Russel and E.E. Bell, Journal of Optical Society America **57**, 23 341 (1967).

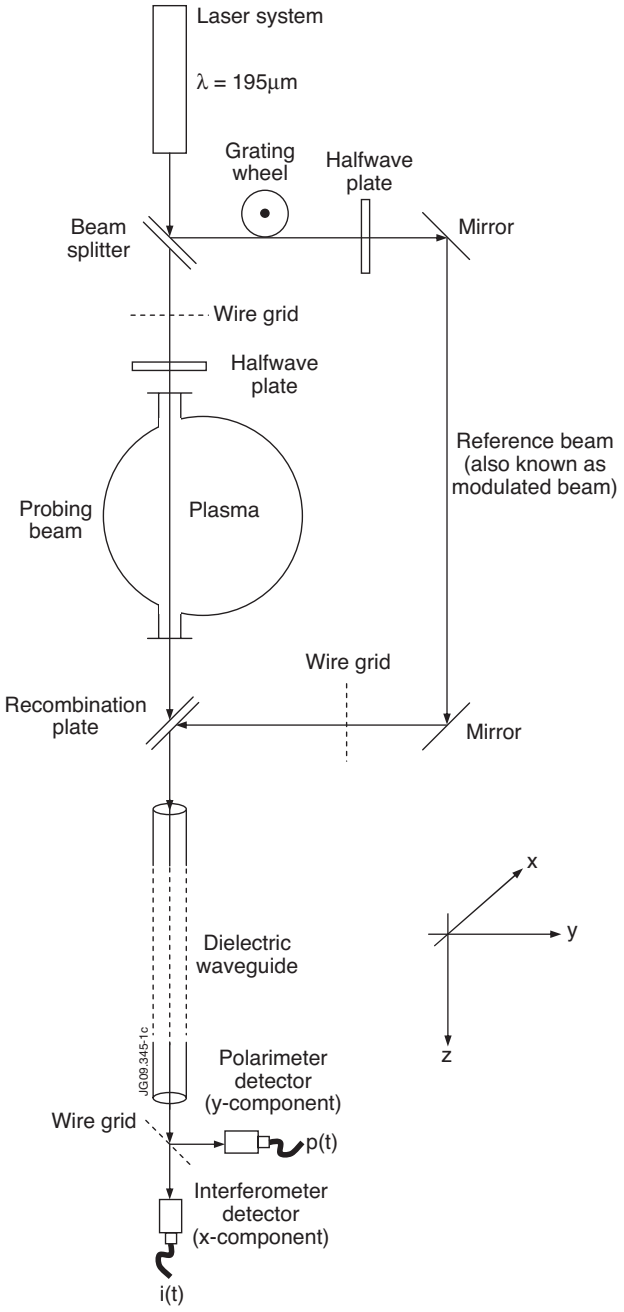

Figure 1: Diagnostic layout for one vertical chord of the polari-interferometer at JET.

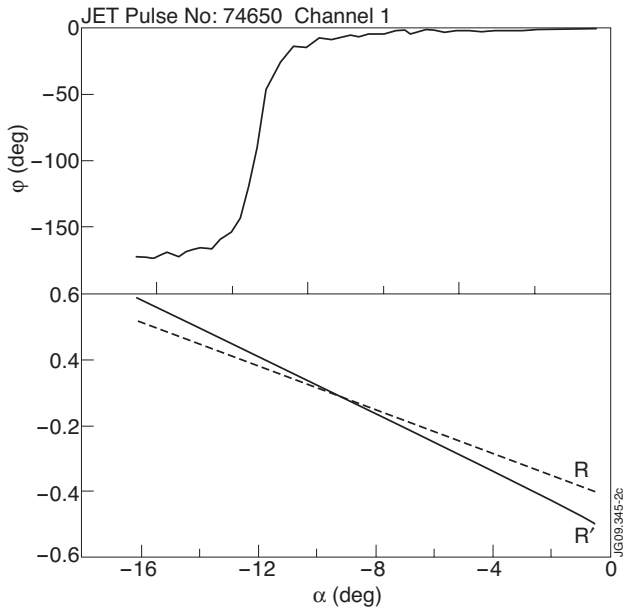

Figure 2: Evolution of φ, R and R′ with respect to the angle α for channel 1.

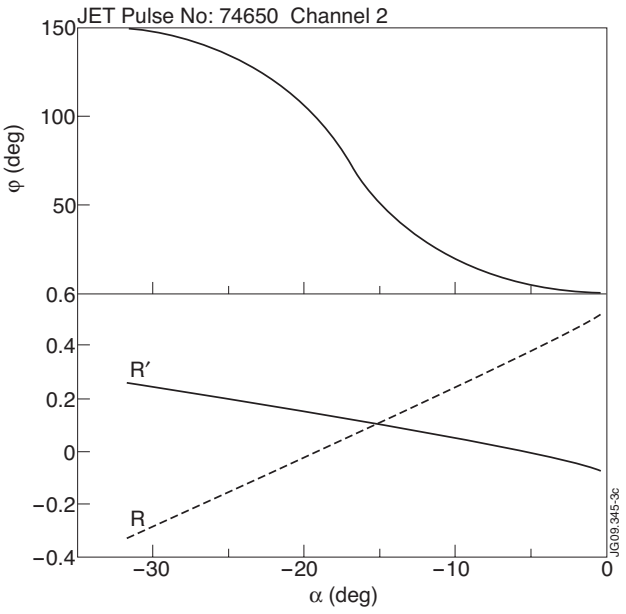

Figure 3: Evolution of φ, R and R′ with respect to the angle α for channel 2.

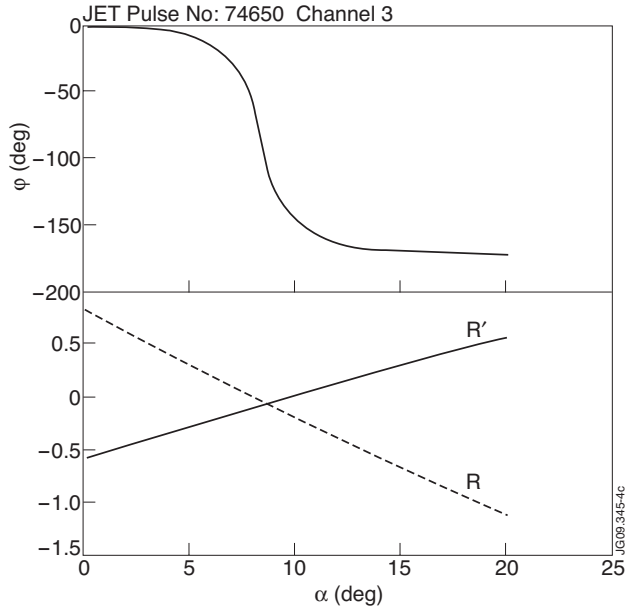

Figure 4: Evolution of φ, R and R′ with respect to the angle α for channel 3.

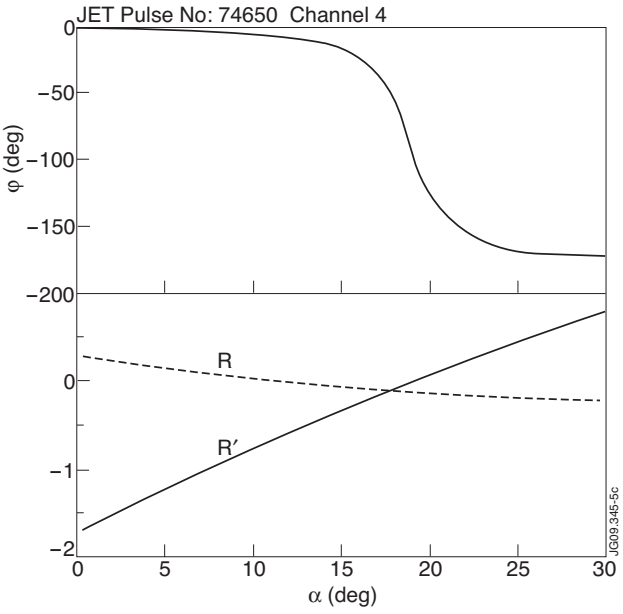

Figure 5: Evolution of φ, R and R′ with respect to the angle α for channel 4.

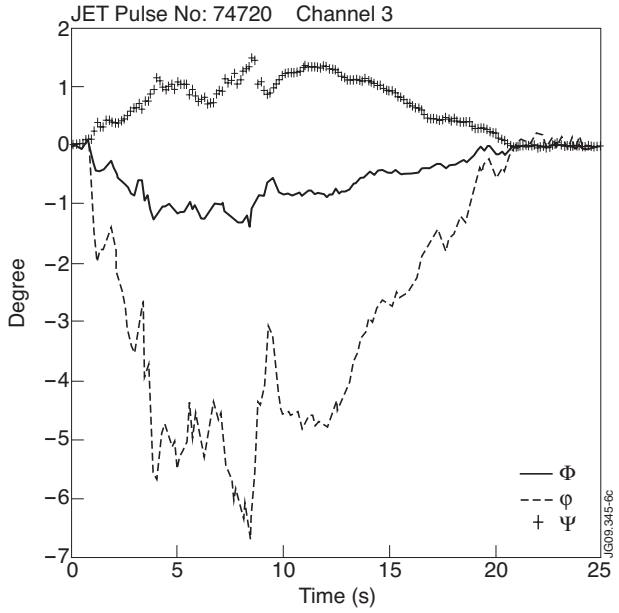

Figure 6: Evolution of Φ, of the Faraday rotation angle Ψ and of the phase shift φ during one shot for channel 3. The signals Φ and Ψ are processed by the software; φ comes directly from the raw data.

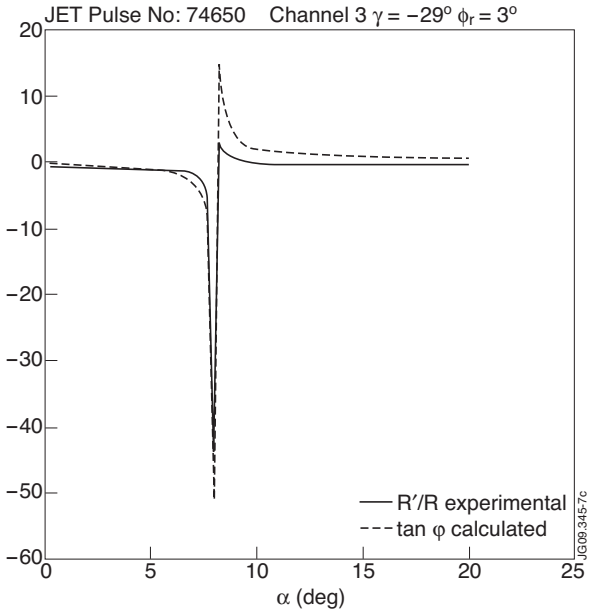

Figure 7: Experimental R′/R curve for channel 3 is compared with theoretical tan φ, calculated with $\gamma = -29^o$ and $\phi_r = 3^o$.